Solid state photodimerization of 9-tert-butyl anthracene ester produces an exceptionally metastable polymorph according to first-principles calculations

Journal:	*CrystEngComm*
Manuscript ID	CE-ART-11-2018-001985.R1
Article Type:	Paper
Date Submitted by the Author:	01-Dec-2018
Complete List of Authors:	Beran, Gregory; University of California Riverside, Chemistry

Journal Name

ARTICLE TYPE

Cite this: DOI: 10.1039/xxxxxxxxxx

Solid state photodimerization of 9-*tert*-butyl anthracene ester produces an exceptionally metastable polymorph according to first-principles calculations.†

Gregory J. O. Beran*[a]

Received Date
Accepted Date

DOI: 10.1039/xxxxxxxxxx

www.rsc.org/journalname

Molecular crystal engineering seeks to tune the material properties by controlling the crystal packing. However, the range of achievable properties is constrained by the limited energy range of polymorphs which can be crystallized. Here, computational modeling highlights that a solid-state crystal-to-crystal chemical reaction in 9-*tert*-butyl anthracene ester (9TBAE) nanorods [Al-Kaysi et al, *J. Am. Chem. Soc.* **128**, 15938 (2006)] imparts "synthetic memory" into the crystal structure that allows reproducible formation of a highly metastable, yet long-lived polymorph. Specifically, whereas the vast majority of known polymorphs exhibit lattice energy differences below 10 kJ/mol, the conformational polymorph formed via solid state reaction chemistry lies 14 kJ/mol higher in energy than the form grown from solution according to calculations that combine a dispersion-corrected second-order Møller-Plesset perturbation theory (MP2D) treatment of the monomer and photodimer with a density functional theory treatment (B86bPBE-XDM) of the intermolecular interactions in the crystal. Moreover, the solid-state reaction environment traps a highly unstable intramolecular photodimer conformation which defies the conventional wisdom surrounding conformational polymorphs. These observations suggest that solid-state reaction chemistry represents an under-appreciated strategy for producing polymorphs that would likely be unobtainable otherwise.

About half of all organic molecules likely exhibit polymorphism in the solid state, meaning they can adopt multiple distinct crystal packing motifs.[1] Changing the crystal packing alters the physical properties of the material, with potentially significant impacts for pharmaceuticals and other organic material applications. Conformational polymorphs, where changes in intramolecular conformation give rise to new intermolecular packing motifs, are particularly likely to exhibit diverse physical properties. Large polarity changes (>1.5 Debye) are an order of magnitude more common in conformational polymorphs than regular polymorphs.[2] The dramatically reduced solubility of the form II conformational polymorph of HIV drug Ritonavir relative to the earlier form I forced the drug's temporary removal from the market.[3] Changes in intramolecular conformation are responsible for the vibrant red, orange, and yellow colors observed across the ten ROY polymorphs.[4] Even seemingly minor chemical modifications to rubrene can alter its solid-state conformation and completely change its carrier mobility.[5,6]

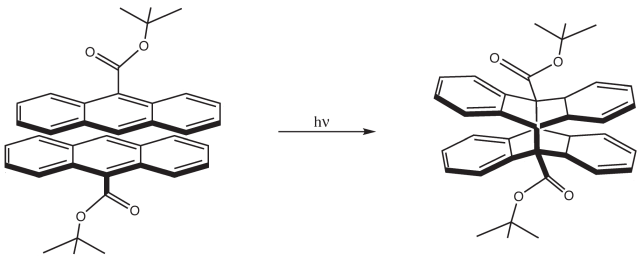

Fig. 1 The [4+4] photodimerization of 9TBAE.

Crystal engineering seeks to achieve desirable material properties by controlling the crystal packing. Unfortunately, the crystal packing that optimizes a given property will often differ from the energetically most stable packing. In specific applications, it may be desirable to target metastable polymorphs to obtain the necessary crystalline properties. However, the variety of polymorphs that can be crystallized and the associated range of achievable physical properties is constrained by the modest energy range of thermodynamically accessible polymorphs. Surveys suggest that half of polymorphs pairs differ by less than 2 kJ/mol in lattice energy, and the vast majority of polymorphs lie within 10 kJ/mol of

[a] *Department of Chemistry, University of California, Riverside, California 92521 USA; E-mail: gregory.beran@ucr.edu*

† Electronic Supplementary Information (ESI) available: Optimized crystal structures, additional details of the MP2D energy refinement, and discussion of the lattice energy differences in other polymorphic crystals. See DOI: 10.1039/b000000x/

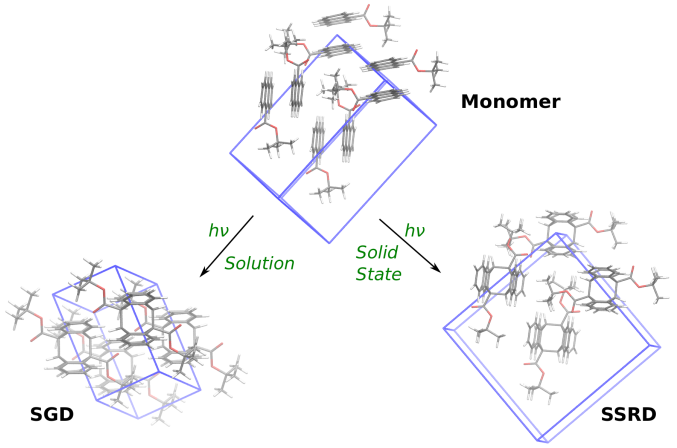

Fig. 2 The solution-grown dimer (SGD) polymorph (CSD RefCode ANODAJ) is formed by photodimerizing 9TBAE monomers (RefCode NUKMIP01) and crystallizing from solution, while the solid-state reacted dimer (SSRD) polymorph is formed via solid-state crystal-to-crystal photodimerization.

the most stable form.[1,7,8] Enlarging the energetic stability window of accessible polymorphs would allow access to new crystal structures which could diversify the corresponding properties that could be achieved. The key to engineering highly metastable forms lies in identifying the experimental conditions under which those structures will be kinetically preferred over the more thermodynamically favored ones.

Here, quantum chemical modeling is used to demonstrate how a solid-state crystal-to-crystal photochemical reaction imparts solid-state "synthetic memory"[2] into the crystal structure that allows reproducible formation of an extraordinarily high-energy polymorph. Specifically, this work focuses on the [4+4] photodimerization of 9-*tert*-butyl anthracene ester (9TBAE) shown in Figure 1 and the polymorphism of the photodimer product. The solid-state photodimerization of this molecule has previously been studied in detail experimentally.[10–12]

In the solid state, 9TBAE molecules pair up as non-covalent dimers, and those dimer pairs pack together in a herringbone fashion (Figure 2). Performing the photodimerization in nanorod crystals of 9TBAE monomers induces photodimerization within each non-covalent dimer pair. This results in formation of the solid state reacted dimer (SSRD) polymorph with a herringbone packing of photodimer molecules.[9] The rapid crystal-to-crystal transition from the monomer to SSRD elongates the nanorods by up to 15%, and by 8±2% on average.[10–12] In contrast, crystallization of the photodimer product from *n*-hexane solution produces the solution grown dimer (SGD) polymorph, with photodimer molecules aligned in parallel one-dimensional stacks.[11] The intramolecular conformation of the photodimers also differs between the SSRD and SGD polymorphs. Whereas the *tert*-butyl ester side chains in the SGD polymorph orient outward relative to the dianthracene core (Figure 3a), they rotate inward in the SSRD form (Figure 3b).

The present study employs quantum chemistry to investigate the energetics of these crystal structures. Whereas the vast majority of known polymorphs exhibit lattice energy differences below 10 kJ/mol, the modeling described here indicates that the SSRD polymorph produced by photodimerization in the nanorods lies ∼14 kJ/mol higher in energy than the SGD one. Moreover, the solid-state photochemical reaction captures a highly unstable intramolecular photodimer conformation in the SSRD which defies conventional wisdom surrounding conformational polymorphs. Despite its highly metastable nature, the SSRD polymorph is long-lived experimentally, converting back to a mixture of monomer and the SGD polymorph over several weeks at room temperature.[11] The insights gained from the electronic structure calculations suggest that solid-state reaction chemistry represents an under-appreciated strategy for producing polymorphs that would likely be unobtainable otherwise.

Results and Discussion

Modeling the polymorphism requires knowledge of the crystal structures. X-ray diffraction structures for the 9TBAE monomer (RefCode NUKMIP01[10]) and SGD (RefCode ANODAJ[11]) are available from the Cambridge Structure Database (CSD).[13] Obtaining the experimental crystal structure of the SSRD proved more challenging.[9,11] The solid-state SSRD polymorph is formed when the photochemical reaction is performed in nanorods, while larger crystals of 9TBAE shatter upon photodimerization. Determination of the structure of the nanorod crystals after photodimerization proved infeasible from powder X-ray diffraction alone. Instead, the structure was solved via a combination of powder diffraction, solid state nuclear magnetic resonance (NMR) spectroscopy, and *ab initio* chemical shift prediction.[9]

Specifically, Ref 9 identified eight candidate structures consistent with the powder X-ray diffraction data. For each of the eight candidates, the unit cell vectors and atomic positions were relaxed and isotropic ^{13}C NMR chemical shifts predicted using density functional theory (DFT). Those simulated chemical shifts were then compared against the experimentally measured ones. In the end, predicted chemical shifts for six of the eight candidate structures agreed well with the experimental NMR, while the chemical shift errors were greater for the other two candidate structures. Analysis of the best six structures indicated that they are closely related via rotations of the *tert*-butyl methyl groups which likely interconvert dynamically at room temperature.[9] Figure 3b shows the similarity in the intramolecular photodimer conformations of the six best structures, while Figure 3c does the same for the other two structures. In all cases, the intermolecular packing is very similar, and the changes in space group result largely from the changes in *tert*-butyl orientations.[9]

To investigate the polymorphism of the photodimer crystals, the present study considers all eight candidate structures once again. This time, however, the focus lies on computing the energetics of these structures using more accurate electronic structure methods and comparing those energetics against the monomer and SGD crystal forms. To begin, the monomer, SGD, and all eight SSRD structures were fully relaxed using planewave DFT and the dispersion-corrected B86bPBE-XDM density functional.[14–16] See the Methods section for computational details. B86bPBE-XDM should be more reliable[17–21] for molecular crystals than the PBE-

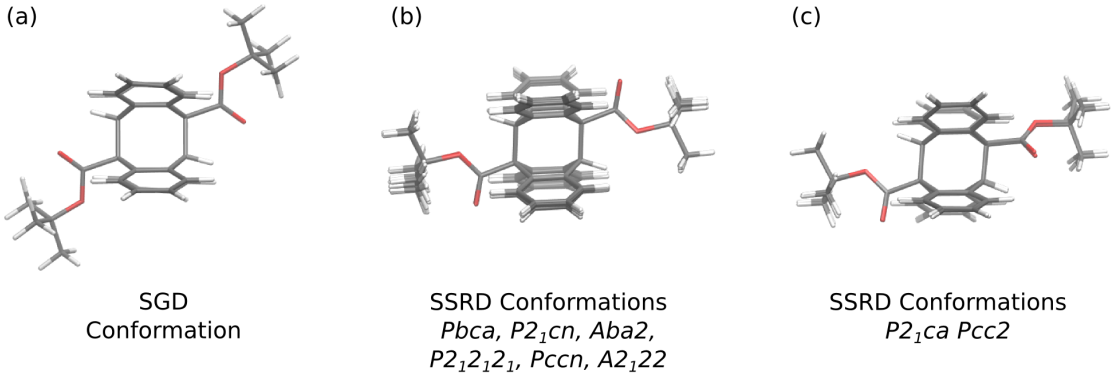

Fig. 3 Comparison of the intramolecular conformations of the photodimer in (a) the SGD polymorph, (b) the six low-energy SSRD structures overlaid, and (c) the two high-energy SSRD structures overlaid. In the SGD the esters orient outward relative to anthracene core, while they orient inward for the SSRD conformations in (b). In (c), the left ester is oriented inward while the right one is oriented at an intermediate angle.

Table 1 Relative energies of the different polymorphs compared to either the SGD form or the unreacted 9TBAE monomer crystal.

Structure	DFT B86bPBE-XDM		MP2D/CBS Refinement	
	Energy vs SGD[a] (kJ/mol)	Energy vs Monomer[b] (kJ/mol)	Energy vs SGD[a] (kJ/mol)	Energy vs Monomer[b] (kJ/mol)
SGD	0.0	81.4	0.0	8.9
SSRD *Pbca*	11.3	92.7	13.3	23.2
SSRD $P2_1cn$	11.1	92.6	13.8	22.7
SSRD *Aba*2	11.3	92.7	14.2	23.1
SSRD $P2_12_12_1$	11.4	92.8	14.2	23.1
SSRD *Pccn*	11.5	92.9	14.4	23.3
SSRD $A2_122$	11.7	93.1	14.4	23.3
SSRD $P2_1ca$	43.4	124.8	45.7	54.6
SSRD *Pcc*2	46.8	128.3	49.0	57.9

[a] Computed as $\Delta E = E_{SSRD} - E_{SGD}$ [b] Computed as $\Delta E = E_{crystal}^{photodimer} - 2E_{crystal}^{monomer}$

D2 density functional/dispersion correction combination used to relax structures in Ref 9.

As shown in Table 1, the six SSRD candidate structures that best matched the NMR data in Ref 9 (*Pbca*, $P2_1cn$, *Aba*2, $P2_12_12_1$, *Pccn*, and $A2_122$) exhibit very similar B86bPBE-XDM energies of 11.4 $\pm$ 0.2 kJ/mol relative to the SGD, consistent with the argument that they are closely related and probably dynamically interconverting. In contrast, the remaining $P2_1ca$ and *Pcc*2 candidate SSRD structures lie ~30-35 kJ/mol higher in energy than the other SSRD candidates, making them unlikely to represent the experimental structure. This assessment is consistent with the earlier NMR work, where the predicted ^{13}C chemical shifts for those two structures exhibited significantly worse agreement with the experimental spectrum.[9] Given the close structural relationships and energetics of the six best structures, all SSRD energies discussed below represent an average over the values for the six structures.

The electronic structure of anthracene photodimerization reactions is notoriously difficult to model correctly[22] due to the strained intramolecular conformation and strong van der Waals π–π interactions in the photodimer. B86bPBE-XDM and many other DFT models incorrectly predict the gas phase photodimer product as being less stable than two non-interacting monomers. The author recently helped develop a dispersion-corrected second-order Møller-Plesset perturbation theory (MP2D) which accurately reproduces benchmark coupled cluster energetics for the anthracene photodimerization reaction and thousands of other benchmark systems.[23] Potential energy curves comparing B86bPBE-XDM and MP2D against coupled cluster singles, doubles, and perturbative triples (CCSD(T)) for anthracene dimerization are provided in ESI.† Those benchmarks demonstrate that MP2D reproduces the CCSD(T) reaction energy for the pure gas phase anthracene photodimerization to within 0.7 kJ/mol.

Because (i) the solid-state photodimer crystals are too large to model with MP2D and (ii) B86bPBE-XDM should describe the intermolecular interactions well, the final energies of the crystals are computed here as the DFT energy of the periodic crystal plus a correction that replaces the DFT treatment of the intramolecular interactions with the more reliable complete-basis-set MP2D one,

$$E_{crystal} = E_{crystal}^{DFT} + \left(E_{intra}^{MP2D} - E_{intra}^{DFT}\right) \quad (1)$$

This strategy is similar to the author's hybrid many-body interaction fragment approach,[24–26] except that only the one-body terms are computed at the higher level of theory instead of both one- and two-body terms.

Applying MP2D to the 9TBAE photodimerization reaction energy lowers the energy of the photodimers versus the monomer crystal by ~70 kJ/mol as compared to B86bPBE-XDM. As shown

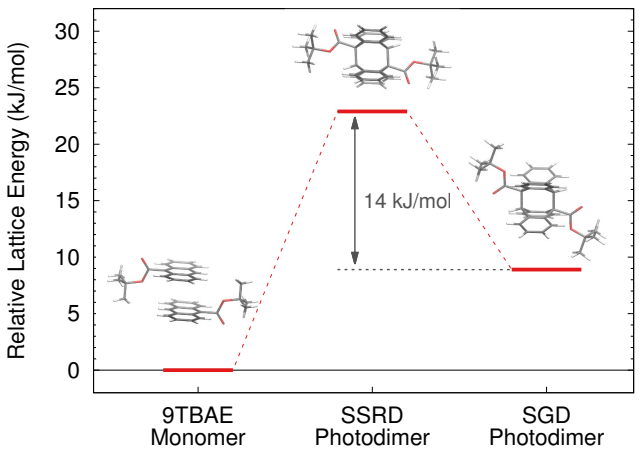

Fig. 4 Lattice energies for SSRD and SGD photodimer (ANODAJ) crystals relative to that of the unreacted monomer crystal (NUKMIP01) at the hybrid MP2D/CBS + B86bPBE-XDM level of theory.

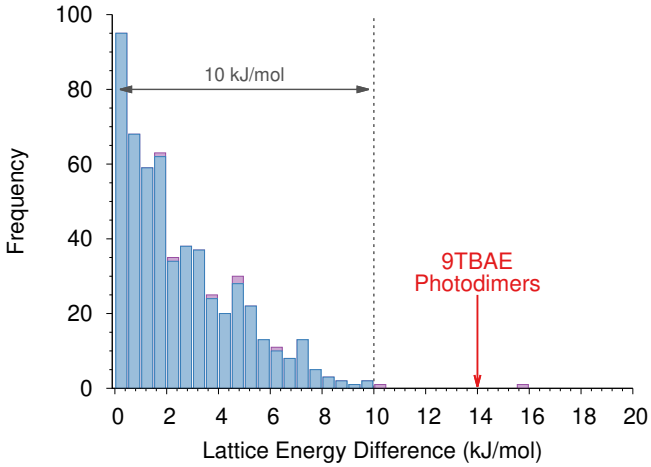

Fig. 5 Comparison of the 14 kJ/mol lattice energy difference for the 9TBAE photodimer polymorphs versus the lattice energy differences for 552 polymorph pairs from the Nyman and Day survey.[7] The distribution plotted here combines the Ref 7 values for the 544 polymorph pairs with lattice energy differences $<$10 kJ/mol (blue) and new periodic B86bPBE-XDM refinement for the eight polymorph pairs which had energy differences $>$10 kJ/mol in Ref 7 (purple).

in Figure 4 and Table 1, the SSRD now lies 23 kJ/mol above the monomer crystal, and more significantly, 14 kJ/mol higher than the SGD polymorph. Further details regarding the intra- and intermolecular contributions provided in ESI.†

While the 14 kJ/mol difference between the SSRD and SGD structures is not the largest lattice energy difference reported between polymorphs, it is exceptionally large. Surveys over hundreds of polymorphic pairs have found that roughly half of polymorphs differ by less than 2 kJ/mol in lattice energy.[1,7,8] 90-95% of polymorphs are separated by no more than ∼6–7 kJ/mol. Conformational polymorphs like those here do tend to exhibit larger energy differences than other polymorphs—one survey found 23% had lattice energy differences between 6–10 kJ/mol, versus only ∼10% of regular polymorphs in the same range.[1]

Nevertheless, lattice energy differences greater than 10 kJ/mol are quite rare. Only eight of the 552 pairwise polymorph comparisons (1.5%) surveyed in Ref 7 exceeded the 10 kJ/mol lattice energy window. That survey computed the energy differences using a hybrid approach that combined DFT for intramolecular conformation and a molecular mechanics force field for the intermolecular interactions. Refinement of the crystal structures and energies for those eight polymorphic pairs at the fully periodic B86bPBE-XDM DFT level of theory here reduces the lattice energy differences in all eight cases appreciably (by an average 7.4 kJ/mol). Only two of the eight pairs retain an energy difference greater than 10 kJ/mol: 3,5-diphenyl-3-amino-1,2,4-triazole at 15.9 kJ/mol, and N,N'-(*p*-phenylene)dibenzamide at 10.5 kJ/mol. See ESI for details.† In other words, the 14 kJ/mol lattice energy difference between the SSRD and SGD here is larger than all but one of those 552 polymorph pairs (Figure 5).

The 9TBAE system also stands out from typical conformational polymorphs for the large energy difference between the intramolecular photodimer conformations in the SGD and SSRD. The two photodimer conformations differ in the orientations of the *tert*-butyl esters relative to the dianthracene core (Figure 3). The outward ester conformation found in the SGD conformation is nearly identical to the gas phase optimized one, while the inward conformation of the SSRD is an unusually large 24 kJ/mol higher in energy (Figure 6). Previous work suggests that about half of flexible molecules adopt a conformation in the solid state that lies within 2.5 kJ/mol (kT at room temperature) of the optimal gas phase conformation, and 90% lie within 10.5 kJ/mol.[2]

Intramolecular conformational energy differences greater than 24 kJ/mol between the gas phase and crystalline conformations are known,[2,27] but 9TBAE defies the conventional wisdom for how such unstable conformations occur. The occurrence of very unstable intramolecular conformations in crystals typically arises from replacing intramolecular non-covalent interactions in the gas phase conformation with intermolecular interactions in the solid state conformation(s). In sugars, for example, gas phase intramolecular hydrogen bonds rearrange to intermolecular hydrogen bonds in the crystal.[2] Large, flexible molecules frequently switch from globular gas phase conformations to extended geometries in the solid state.[27] Indeed, a direct correlation has been demonstrated between the relative instability of the intramolecular conformation adopted in a crystal and the increase in the surface area of that conformation relative to the gas phase one.[27]

The highly unstable intramolecular conformation found in the SSRD polymorph does not adhere to either mechanism: it forms no hydrogen bonds, and the Connolly surface area[28] of the SSRD photodimer conformer (462 Å^2) is actually 1% smaller than the SGD one/gas phase one (467 Å^2), not larger as the conventional wisdom would suggest. Instead, the strained intramolecular conformation in the SSRD polymorph arises from topochemical principles—the solid-state photochemical reaction forms the dimer with the unfavorable orientations of the *tert*-butyl ester groups, and the dense crystal packing inhibits their intramolecular relaxation. The photons provide the energy input required to access the highly metastable polymorph, and forming the poly-

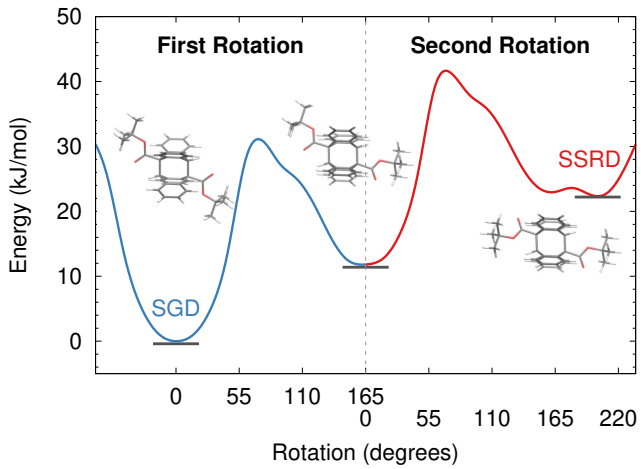

Fig. 6 Gas phase energy profile for converting the 9TBAE photodimer from the SGD-like to SSRD-like conformations via sequential *tert*-butyl ester group rotations at the MP2D/CBS limit level of theory. The SSRD conformation lies 24 kJ/mol above the SGD one, with a 41 kJ/mol kinetic barrier between them.

morph via solid-state chemistry preserves the synthetic memory of the monomer crystal packing.

This immediately raises the question: might one be able to crystallize the SSRD directly from solution-phase photodimers, without invoking the solid-state chemical reaction? While one should not rule out experimental ingenuity, it seems unlikely. In the gas phase, the intramolecular conformation adopted by the SSRD is 24 kJ/mol less stable than the SGD one, and a 41 kJ/mol kinetic barrier separates the SSRD conformation from the more stable SGD one (Figure 6). Furthermore, there is little energetic driving force to crystallize into the SSRD polymorph. Compared to the SGD, the more optimal SSRD crystal packing only restores 10 kJ/mol of the 24 kJ/mol penalty incurred by adopting that unfavorable intramolecular conformation (leading to the net 14 kJ/mol difference between SGD and SSRD polymorphs).

These results demonstrate that solid-state reactions can facilitate the preparation of long-lived, highly metastable crystal polymorphs. Solution-phase synthetic memory is already recognized as a means for accessing polymorphs of kinetically inaccessible intramolecular conformations.[2] For example, different solution-phase syntheses can produce either the *syn* or *anti* conformers of a bis-urea macrocycle.[29,30] Though the stability difference between the two conformers is modest,[2] the barrier to interconversion is high[30] and the synthesized conformation is retained upon crystallization to produce two distinct polymorphs. Similarly, a fluorinated hexabenzocoronene can be synthesized in a metastable conformation which reverts to the stable conformation above 100°C, allowing for straightforward crystallization of either conformer.[31]

Desolvation after crystallization provides another strategy for retaining memory of precursor structure.[32] In one recent notable example,[33] highly porous organic molecular structures formed from triptycene derivatives were more stable than the densely packed polymorph as long as the pores were filled with solvent. Upon desolvation, however, force field calculations indicate that the porous structures become up to ~50 kJ/mol less stable than the densely packed one.

In contrast, the use of solid-state synthetic memory to retain crystal packing features from the reactant(s) in the product crystal has not been widely exploited in crystal engineering. This phenomenon is not unique to the 9TBAE system. Other examples of metastable crystal forms being formed through solid-state photochemistry can be found in the literature. For example, the *p*-nitrosobenzene polymorph formed via solid-state photochromic dissociation of the dimer is metastable relative the polymorph formed directly from monomer sublimation (by ~4 kJ/mol, see ESI†) and survives below 170 K.[34] The photodimerization of *ortho*-ethoxy-*trans*-cinnamic acid produces a 1:1 ordered co-crystal of truxilic acid and unreacted monomer[35] which is 10.3 kJ/mol less stable than crystals of the pure components.[36] Given the diversity of solid-state chemical reactions,[37–39] many more examples can likely be found in existing studies which did not examine the polymorphism of the products. In some cases, the metastable phase formed by the reaction may be short-lived and ill-characterized,[40] but in many others they should be sufficiently stable to study.

The fundamental challenge will be to devise solid-state reactions which preserve crystallinity and for which the product polymorphs are long-lived despite their metastability. Many photochemical reactions in single crystals shatter under the strain created by the product, for example, though this strain can be alleviated in nanoscale crystals.[39] Might those nanocrystals subsequently provide useful seeds for growing macroscopic crystals of the metastable form?

The most obvious approach to achieve long-lived, highly metastable polymorphs would be to exploit reactions that produce strained intramolecular conformations for which the solid-state relaxation barriers will likely be large. In 9TBAE, relaxation from the SSRD conformation to the SGD one would occur readily in solution, but it is hindered in the solid state by the need to rotate bulky *tert*-butyl ester side chains. While identifying reactants with the correct crystal packing can be challenging, solid state synthetic memory also has advantages: it should prove easier to trap highly strained conformations in densely packed solids compared to in solution.

Conclusions

In summary, computational modeling demonstrates that the polymorph of 9TBAE photodimers formed via solid state reaction is an exceptionally large 14 kJ/mol less stable than the crystal form obtained via solution-phase crystallization, and that the metastable form also adopts a highly strained intramolecular conformation. While the vast majority molecular crystal polymorphs generally lie within a 10 kJ/mol energy window of the most stable crystal form, this 9TBAE photodimer example highlights how creative use of "memory" from precursor structures can be exploited to enlarge the energy window and produce otherwise unobtainable crystal forms. Solid state reaction chemistry is increasingly used to synthesize target molecules, but much less attention has been paid to how it can be used to produce specific crystal structures. The results here suggest that solid state synthetic memory could

provide a potentially interesting tool for engineering new crystal polymorphs with unusual properties.

Computational Methods

Unit cell vectors and atomic positions for all crystal structures were relaxed with planewave density functional theory using the B86bPBE density functional[14,15] and the XDM dispersion correction[16] as implemented in Quantum Espresso.[41,42] A planewave energy cutoff of 50 Ry and *k*-point grid of 3×1×3 for the monomer, 3×3×3 for the SGD, and either 1×3×1 or 1×1×3 for the SSRD candidates (depending on the whether the short cell vector as in the b or c direction). PAW potentials for the atoms were produced using A. Dal Corso's Atomic code v6.1. The optimizations started from experimental crystal structures (or for the SSRD, the eight candidate crystal structures from Ref 9.

Next, the energies were refined at the MP2D level. Because fully computing the crystal energies with MP2D would be computationally prohibitive, the MP2D crystal energetics were approximated according to Eq 1. The primary problem with the DFT results here stems from the intramolecular description of the very short-range van der Waals interactions coupled with the large energy changes associated with small changes in the anthracene ring distortion and inter-ring separation in the photodimer. This hybrid approach corrects the description of those intramolecular interactions at the MP2D level, while retaining the B86bPBE-XDM treatment of the intermolecular ones. To evaluate Eq 1, the DFT energies of the 9TBAE monomer or photodimer molecules was computed in a large periodic box with 15 Å of vacuum spacing in all three Cartesian directions and a 1×1×1 *k*-point grid. The MP2D energetics were computed at the complete basis set limit via two-point extrapolation[43] of the correlation energy computed in the def2-TZVP and def2-QZVP basis sets.[44] The density-fitted MP2 calculations were performed with a developmental version of PSI4[45] that includes the new dispersion correction.

The torsional energy profile plotted in Figure 6 was computed by performing constrained energy scans. Starting from the SSRD conformation, the dihedral angle of one *tert*-butyl ester group relative to its anthracene ring was constrained at a given angle, and all other degrees of freedom were optimized. After mapping out the energy profile for the first rotation and identifying the optimal SGD-like torsion angle, the energy profile generated by rotating the second *tert*-butyl ester group was generated similarly. The combination of these two scans produces Figure 6. These constrained optimizations were performed using Gaussian 09.[46] Because B86bPBE-XDM is not well integrated into Gaussian, the geometry optimizations were performed with B3LYP-D3(BJ)/def2-TZVP. The final energetics plotted were then obtained from single-point MP2D/CBS energy calculations on the DFT geometries.

Conflicts of interest

There are no conflicts to declare.

Acknowledgments

Funding from the National Science Foundation (CHE-1665212) and computing resources from XSEDE (TG-CHE110064) are gratefully acknowledged. Sally Price, Christopher Bardeen, Graeme Day, and Leonard Mueller are thanked for the stimulating discussions that led to this work.

References

1 A. J. Cruz-Cabeza, S. M. Reutzel-Edens and J. Bernstein, *Chem. Soc. Rev.*, 2015, **44**, 8619–8635.
2 A. J. Cruz-Cabeza and J. Bernstein, *Chem. Rev.*, 2014, **114**, 2170–2191.
3 J. Bauer, S. Spanton, R. Quick, J. Quick, W. Dziki, W. Porter and J. Morris, *Pharm. Res.*, 2001, **18**, 859–866.
4 L. Yu, *Acc. Chem. Res.*, 2010, **43**, 1257–66.
5 S. Haas, A. F. Stassen, G. Schuck, K. P. Pernstich, D. J. Gundlach, B. Batlogg, U. Berens and H. J. Kirner, *Phys. Rev. B*, 2007, **76**, 115203.
6 C. Sutton, M. S. Marshall, C. D. Sherrill, C. Risko and J.-L. Brédas, *J. Am. Chem. Soc.*, 2015, **137**, 8775–8782.
7 J. Nyman and G. M. Day, *CrystEngComm*, 2015, **17**, 5154–5165.
8 A. Burger and R. Ramberger, *Mikrochim. Acta*, 1979, **72**, 273–316.
9 C. Yang, L. Zhu, R. A. Kudla, J. D. Hartman, R. O. Al-Kaysi, S. Monaco, B. Schatschneider, A. Magalhaes, G. J. O. Beran, C. J. Bardeen and L. J. Mueller, *CrystEngComm*, 2016, **18**, 7319–7329.
10 R. O. Al-Kaysi, A. M. Müller and C. J. Bardeen, *J. Am. Chem. Soc.*, 2006, **128**, 15938–15939.
11 L. Zhu, A. Agarwal, J. Lai, R. O. Al-Kaysi, F. S. Tham, T. Ghaddar, L. Mueller and C. J. Bardeen, *J. Mater. Chem.*, 2011, **21**, 6258–6268.
12 R. Kudla, L. Zhu, C. Yang, X. Dong, F. Tong, K. Chalek, R. O. Al-Kaysi, J. D. Hartman, F. S. Tham, G. J. O. Beran, C. J. Bardeen and L. J. Mueller, *in preparation*, 2018.
13 C. R. Groom, I. J. Bruno, M. P. Lightfoot and S. C. Ward, *Acta Cryst. B*, 2016, **72**, 171–179.
14 A. D. Becke, *J. Chem. Phys.*, 1986, **38**, 7184–7187.
15 J. P. Perdew, K. Burke and M. Ernzerhof, *Phys. Rev. Lett.*, 1996, **77**, 3865.
16 A. Otero-de-la Roza and E. R. Johnson, *J. Chem. Phys.*, 2012, **136**, 174109.
17 A. Otero-de-la Roza and E. R. Johnson, *J. Chem. Phys.*, 2012, **137**, 054103.
18 A. Otero-De-La-Roza, B. H. Cao, I. K. Price, J. E. Hein and E. R. Johnson, *Angew. Chem. Int. Ed.*, 2014, **53**, 7879–7882.
19 S. R. Whittleton, A. Otero-de-la Roza and E. R. Johnson, *J. Chem. Theory Comput.*, 2017, **13**, 441–450.
20 S. R. Whittleton, A. Otero-de-la Roza and E. R. Johnson, *J. Chem. Theory Comput.*, 2017, **13**, 5332–5342.
21 J. L. McKinley and G. J. O. Beran, *Faraday Disc.*, 2018, **211**, 181–207.
22 S. Grimme, C. Diedrich and M. Korth, *Angew. Chem. Int. Ed.*, 2006, **45**, 625–629.
23 J. Řezáč, C. Greenwell and G. J. O. Beran, *J. Chem. Theory Comput.*, 2018, **14**, 4711–4721.
24 G. J. O. Beran and K. Nanda, *J. Phys. Chem. Lett.*, 2010, **1**, 3480–3487.
25 G. J. O. Beran, J. D. Hartman and Y. N. Heit, *Acc. Chem. Res.*, 2016, **49**, 2501–2508.
26 G. J. O. Beran, *Chem. Rev.*, 2016, **116**, 5567–5613.
27 H. P. G. Thompson and G. M. Day, *Chem. Sci.*, 2014, **5**, 3173–3182.
28 M. L. Connolly, *J. Appl. Cryst.*, 1983, **16**, 548–558.
29 M. F. Lappert, S. Álvarez, G. Aullón, R. Fandos, A. Otero, A. Rodríguez, S. Rojas and P. Terreros, *Eur. J. Inorg. Chem.*, 2009, **2009**, 1851–1860.
30 W. F. de Souza, N. Kambe, Z. J. Jin, N. Kanehisa, Y. Kai and N. Sonoda, *J. Org. Chem.*, 1995, **60**, 7058–7062.
31 Y.-L. Loo, A. M. Hiszpanski, B. Kim, S. Wei, C.-Y. Chiu, M. L. Steigerwald and C. Nuckolls, *Org. Lett.*, 2010, **12**, 4840–4843.
32 S. Bhattacharya and B. K. Saha, *Crys. Growth Des.*, 2013, **13**, 606–613.
33 A. Pulido, L. Chen, T. Kaczorowski, D. Holden, M. A. Little, S. Y. Chong, B. J. Slater, D. P. McMahon, B. Bonillo, C. J. Stackhouse, A. Stephenson, C. M. Kane, R. Clowes, T. Hasell, A. I. Cooper and G. M. Day, *Nature*, 2017, **543**, 657–664.
34 I. Halasz, E. Mestrovic, H. Cicak, Z. Mihalic and H. Vancik, *J. Org. Chem.*, 2005, **70**, 8461–8467.
35 M. A. Fernandes and D. C. Levendis, *Acta Cryst. B*, 2004, **60**, 315–324.
36 C. R. Taylor and G. M. Day, *Cryst. Growth Des.*, 2018, **18**, 892–904.
37 L. R. MacGillivray, G. S. Papaefstathiou, T. Friscić, T. D. Hamilton, D.-K. Bucar, Q. Chu, D. B. Varshney and I. G. Georgiev, *Acc. Chem. Res.*, 2008, **41**, 280–91.
38 G. Kaupp, *Organic Solid-State Reactions*, 2016, http://doi.wiley.com/10.1002/9781118468586.epoc2005.
39 P. Naumov, S. Chizhik, M. K. Panda, N. K. Nath and E. Boldyreva, *Chem. Rev.*, 2015, **115**, 12440–12490.
40 T. Kim, L. Zhu, L. J. Mueller and C. J. Bardeen, *CrystEngComm*, 2012, **14**, 7792–7799.
41 P. Giannozzi, S. Baroni, N. Bonini, M. Calandra, R. Car, C. Cavazzoni, D. Ceresoli, G. L. Chiarotti, M. Cococcioni, I. Dabo, A. Dal Corso, S. de Gironcoli, S. Fabris, G. Fratesi, R. Gebauer, U. Gerstmann, C. Gougoussis, A. Kokalj, M. Lazzeri, L. Martin-Samos, N. Marzari, F. Mauri, R. Mazzarello, S. Paolini, A. Pasquarello, L. Paulatto, C. Sbraccia, S. Scandolo, G. Sclauzero, A. P. Seitsonen, A. Smogunov, P. Umari and R. M. Wentzcovitch, *J. Phys. Condens. Mat.*, 2009, **21**, 395502.
42 P. Giannozzi, O. Andreussi, T. Brumme, O. Bunau, M. Buongiorno Nardelli, M. Calandra, R. Car, C. Cavazzoni, D. Ceresoli, M. Cococcioni, N. Colonna,

I. Carnimeo, A. Dal Corso, S. de Gironcoli, P. Delugas, R. A. DiStasio, A. Ferretti, A. Floris, G. Fratesi, G. Fugallo, R. Gebauer, U. Gerstmann, F. Giustino, T. Gorni, J. Jia, M. Kawamura, H.-Y. Ko, A. Kokalj, E. Küçükbenli, M. Lazzeri, M. Marsili, N. Marzari, F. Mauri, N. L. Nguyen, H.-V. Nguyen, A. Otero-de-la Roza, L. Paulatto, S. Poncé, D. Rocca, R. Sabatini, B. Santra, M. Schlipf, A. P. Seitsonen, A. Smogunov, I. Timrov, T. Thonhauser, P. Umari, N. Vast, X. Wu and S. Baroni, *J. Phys. Condens. Mat.*, 2017, **29**, 465901.

43 T. Helgaker, W. Klopper, H. Koch and J. Noga, *J. Chem. Phys.*, 1997, **106**, 9639–9646.

44 F. Weigend and R. Ahlrichs, *Phys. Chem. Chem. Phys.*, 2005, **7**, 3297–3305.

45 R. M. Parrish, L. A. Burns, D. G. A. Smith, A. C. Simmonett, A. E. DePrince, E. G. Hohenstein, U. Bozkaya, A. Y. Sokolov, R. Di Remigio, R. M. Richard, J. F. Gonthier, A. M. James, H. R. McAlexander, A. Kumar, M. Saitow, X. Wang, B. P. Pritchard, P. Verma, H. F. Schaefer, K. Patkowski, R. A. King, E. F. Valeev, F. A. Evangelista, J. M. Turney, T. D. Crawford and C. D. Sherrill, *J. Chem. Theory Comput.*, 2017, **13**, 3185–3197.

46 M. J. Frisch, G. W. Trucks, H. B. Schlegel, G. E. Scuseria, M. A. Robb, J. R. Cheeseman, G. Scalmani, V. Barone, B. Mennucci, G. A. Petersson, H. Nakatsuji, M. Caricato, X. Li, H. P. Hratchian, A. F. Izmaylov, J. Bloino, G. Zheng, J. L. Sonnenberg, M. Hada, M. Ehara, K. Toyota, R. Fukuda, J. Hasegawa, M. Ishida, T. Nakajima, Y. Honda, O. Kitao, H. Nakai, T. Vreven, J. A. Montgomery, Jr., J. E. Peralta, F. Ogliaro, M. Bearpark, J. J. Heyd, E. Brothers, K. N. Kudin, V. N. Staroverov, R. Kobayashi, J. Normand, K. Raghavachari, A. Rendell, J. C. Burant, S. S. Iyengar, J. Tomasi, M. Cossi, N. Rega, J. M. Millam, M. Klene, J. E. Knox, J. B. Cross, V. Bakken, C. Adamo, J. Jaramillo, R. Gomperts, R. E. Stratmann, O. Yazyev, A. J. Austin, R. Cammi, C. Pomelli, J. W. Ochterski, R. L. Martin, K. Morokuma, V. G. Zakrzewski, G. A. Voth, P. Salvador, J. J. Dannenberg, S. Dapprich, A. D. Daniels, Ö. Farkas, J. B. Foresman, J. V. Ortiz, J. Cioslowski and D. J. Fox, *Gaussian 09 Revision E.01*, 2009, Gaussian Inc. Wallingford CT.

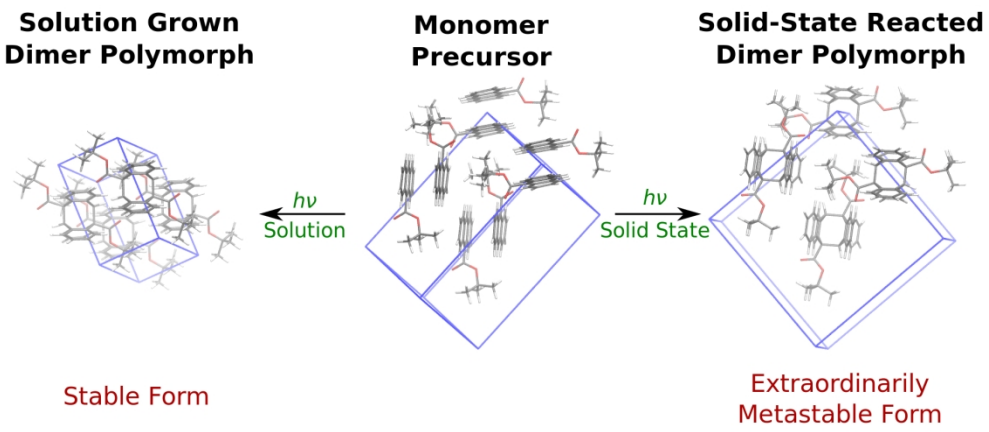
Solution Grown
Dimer Polymorph
Monomer
Precursor
Solid-State Reacted
Dimer Polymorph
hν
Solution
hν
Solid State
Stable Form
Extraordinarily
Metastable Form